PSFC/JA-00-42

AC Loss Measurements of Sub-sized Nb_3Sn CICC Cable with Transport Current

Tim D. Alvey, Makoto Takayasu, and Joseph V. Minervini

December 1, 2000

Plasma Science and Fusion Center
Massachusetts Institute of Technology
Cambridge MA 02139 USA

This work was originally presented at ASC 2000. This work was supported in part by the U.S. Department of Energy, Office of Fusion Energy Science under Grant Number: DE-FG02-93-ER54186. A portion of this work was performed at the National High Magnetic Field Laboratory, Florida State University, which is supported by NSF Cooperative Agreement No. DMR-9527035.

Abstract

An experimental study of AC losses was carried out on a 36-strand sub-sized Cable-In-Conduit-Conductor of Nb_3Sn superconducting wires used for the International Thermonuclear Experimental Reactor (ITER) Central Solenoid model coils. Ripple field loss tests were performed using the 20 T large bore magnet at the National High Field Magnet Laboratory. Small amplitude, sinusoidal ripple field of 4 Hz, superimposed on a DC magnetic field was produced by modulating the magnet power supply. AC losses were measured with transport currents ranging from 0 to 6 kA at various DC background fields up to 12 T using an isothermal calorimetric method. The inter-strand coupling loss of the 36-strand cable increased gradually and then sharply at approximately 30 kN/m with increasing Lorentz force, and resulted in an 84% increase at the Lorentz force of 50 kN/m. The cable coupling current effective time constant ($n_s t_s$) at zero current declined from 20 ms to 8 ms after cyclic Lorentz force loading.

I. INTRODUCTION

An experimental study of energy dissipation, also know as AC loss, was carried out on a 36 strand Cable-In-Conduit-Conductor (CICC). Understanding AC loss mechanisms is one of the most fundamental issues associated with the design of large-scale superconducting magnet systems. This work focuses on measuring AC losses of a sub-sized cable sample in operating with transport currents in DC background fields with a ripple field, in order study inter-strand (strand-strand) coupling loss of Nb_3Sn CICC magnets such as ITER Central Solenoid model coil magnet [1].

AC losses, of the sub-sized cable with and without transport current, were measured using an isothermal calorimetric method. A test probe, used to mount the brittle Nb_3Sn CICC sample and calorimetry system, was designed and fabricated capable of delivering transport currents up to 10 kA to the sample in background magnetic fields ranging from 0 to 20 T.

AC losses produced in the test sample were dominated by inter-strand coupling loss. In order to analyze the effects of the transport currents and the fields on the inter strand coupling loss, hysteresis loss and inter-strand coupling loss were evaluated using previously measured strand data and existing theoretical formulas.

II. EXPERIMENTAL

A calorimetric test probe was designed and constructed to measure AC losses of a 36 strand CICC with and without transport current. The calorimetric test system used a calibration heater (20 m of stainless steel wire wound non-inductively) mounted near the test sample, which was continuously energized to maintain a desired, constant liquid helium boil-off rate at 4.2 K [2], [3]. When the test sample is exposed to an AC field, the sample produces heat generated by the losses and this heat adds to the boil off rate. The increased boil off rate causes a corresponding increase in the measured helium gas by the mass flow meter. The flow meter output signal is used as a feedback signal into a feed back control system which drops the heater power to maintain the original desired flow level. The reduction of the heater power during the automatic control is equal to the amount of heat produced from AC losses. This type of control reduces the equilibration time of each measurement, which is normally

quite long for traditional isothermal calorimetry experiments and greatly increases the accuracy of measurement due to effectively canceling out background changes. The sensitivity of this system was about 2 mW. AC loss signals measured during this experiment varied from 15 mW to 60 mW.

The test sample of total 7 m long including joints, shown in Fig. 1a, is a CICC type with Incoloy Alloy 905 conduit, and a cable made from 36 strands of ITER IGC Nb_3Sn superconducting wire twisted in a 3x3x4 cabling pattern. The conductor information is given in Table I. The cabling twist pitches were 50, 100, and 150 mm for each cabling stage respectively. The coil section, which acted as the test section, was approximately 5 m wound non-inductively with a coil of 83 mm ID and a conduit diameter of 16 mm.

TABLE I

TESTED CONDUCTOR PARAMETERS

STRAND		CABLE	
Superconductor	Nb_3Sn	Number Strands	36
Diameter	0.81 mm	Cabling Configuration	3x3x4
Twist Pitch	9 mm	Cable Twist Pitches: 1^{st}, 2^{nd}, 3^{rd}	50, 100, 150 mm
Strand Insulation	2.3 μm Cr	Conduit Material	Incoloy 905
Copper:Non-copper	1.45	Void Fraction	about 36.5%
RRR	120	Length in Calorimeter	5 m

Following heat treatment, the Nb_3Sn sample was mounted on its sample holder, shown in Fig. 1b, and then assembled into the calorimeter. The calorimeter, shown in Fig. 2, was made from two parts of G10 structures consisting of a 520 mm long, 140 mm OD, 6.4 mm wall thickness tube and an equivalent diameter 76 mm long top piece. A long thin walled G10 tube is connected to the calorimeter top piece, which sends the boiled off helium gas from the calorimeter through a heat exchanger, located outside the cryostat, and finally to the gas measuring system. As shown in Fig. 2, the sample leads were terminated by exiting the leads from the bottom of the calorimeter and then running the leads up the side of the calorimeter to the bus bar termination section, where they were soldered. Exiting from the bottom of the calorimeter allowed to minimize the complexity of the calorimeter top cover and to minimize thermal conduction from the 10 kA vapor cooled current leads.

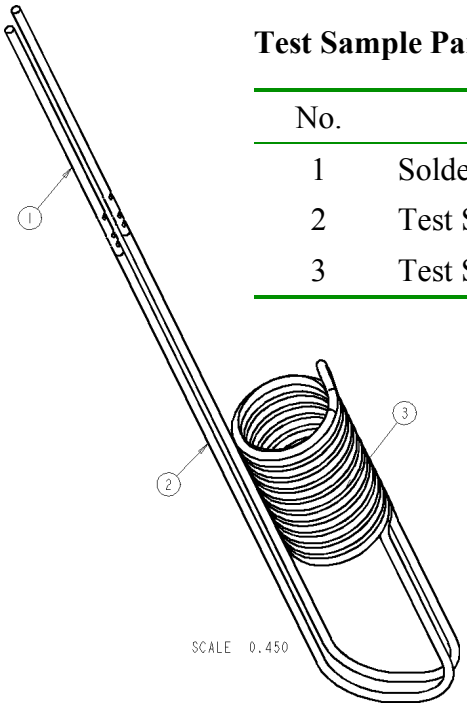

(a)

Test Sample Parts.

No.	Component
1	Solder Filled OFHC Cu Lead Terminations
2	Test Sample Leads
3	Test Sample Section

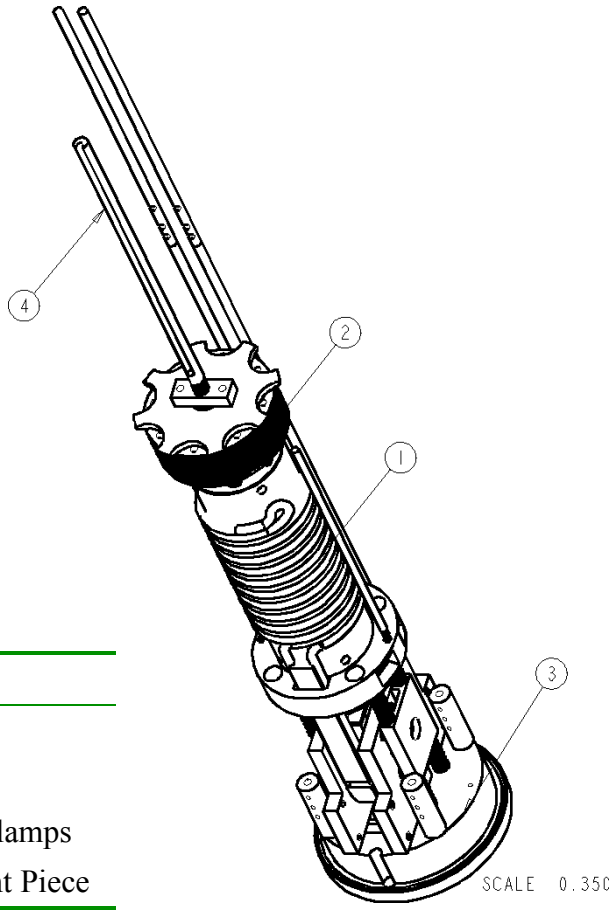

Sample Holder Components.

No.	Component
1	Test Sample
2	Calibration Heater Mount
3	Sample Base and Exit Lead Clamps
4	Liquid He Level Sensor Mount Piece

(b)

Fig. 1. (a) Test Sample – The labeled components are 1) Solder Filled OFHC Cu Lead Terminations, 2) Test Sample Leads and 3) Test Sample Section. (b) Sample Holder – The labeled components are 1) Test Sample, 2) Calibration Heater Mount, 3) Sample Base and Exit Clamps, and 4) Liquid He Level Sensor Mount.

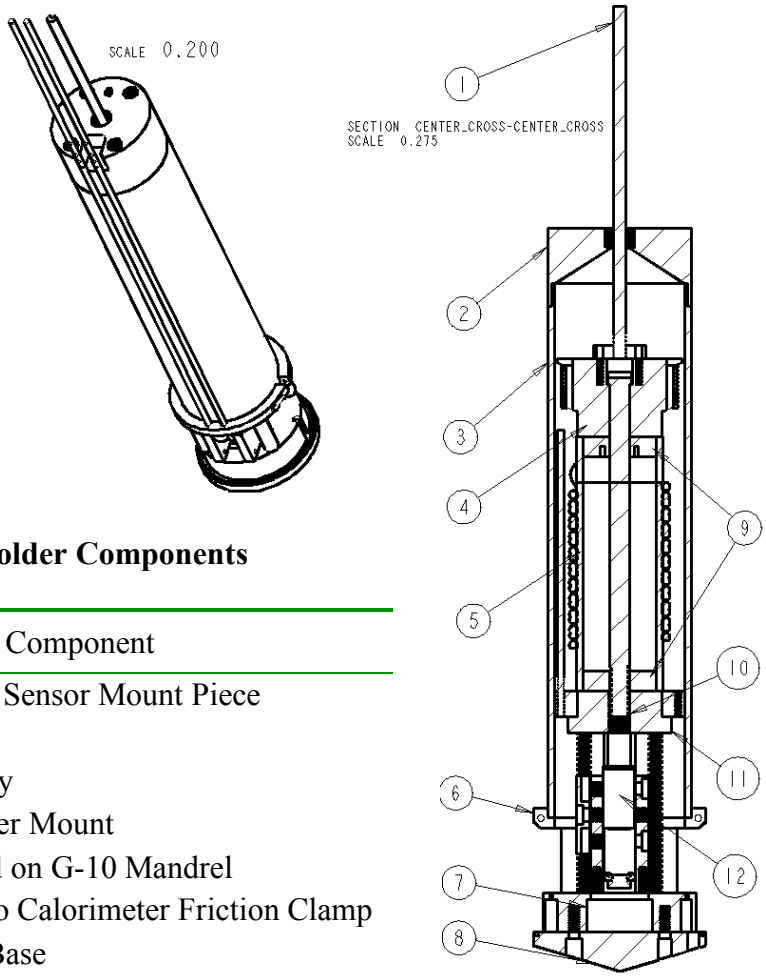

Calorimeter and Sample Holder Components

No.	Component
1	Liquid He Level Sensor Mount Piece
2	Calorimeter Top
3	Calorimeter Body
4	Calibration Heater Mount
5	Sample Mounted on G-10 Mandrel
6	Sample Holder to Calorimeter Friction Clamp
7	Sample Holder Base
8	Sample Holder Gas Diverter and Test Probe
9	Calibration Heater and Sample Mandrel
10	Sample Mandrel Alignment and Hold Down
11	Sample Mandrel Base
12	Exit Lead Spacers and Clamps

Fig. 2 The left view shows an assembly drawing of the sampler holder mounted in the calorimeter. The right view shows a cross-sectional view of the calorimeter assembly.

Experiments were performed using the 20 T, 195 mm diameter warm bore magnet at the National High Field Magnet Laboratory (NHMFL), Florida State University in Tallahassee Florida. The AC field used to produce AC losses in the test sample was generated by modulating the 20 T magnet power supplies in order to create a small amplitude, sinusoidal ripple field superimposed on a DC bias field. Sample transport currents of up to 10 kA could be achieved using one of the four NHMFL facilities of

10 MW magnet power supplies. AC losses were measured as a function of background field, with transport current levels ranging from 0 to 6 kA, at a constant ripple amplitude and a constant frequency.

III. EXPERIMENTAL DATA ANALYSIS METHOD

A. Theoretical background

When an AC magnetic field of B_{max} sin (ωt) is applied to a superconducting wire cable, AC losses in general are comprised of contributions from hysteresis loss and inter-filament coupling loss in a strand, and inter-strand coupling loss among strands. The AC losses Q_T are given as [4]:

$$Q_T = Q_{hys} + Q_{if} + Q_{is} \tag{1}$$

where Q_{hys}, Q_{if}, and Q_{is} are respectively hysteresis loss, inter-filament, and the inter-strand coupling losses.

The expected hysteresis loss component was calculated using [5]:

$$Q_{hys} = \frac{2}{3\mu_o} B_p^2 \left(\frac{B_{max}}{B_p} \right)^3 \qquad (B_{max} \leq B_p)$$

$$Q_{hys} = \frac{2}{\mu_o} B_{max} B_p \left(1 - \frac{2B_p}{3B_{max}} \right)^3 \qquad (B_{max} > B_p) \tag{2}$$

here,

$$B_p = \mu_o J_c a \tag{3}$$

where B_p is the filament penetration field, μ_0 is the permeability of free space ($4\pi 10^{-7}$ H/m), J_c is the critical current, and a is the effective filament radius.

The coupling loss terms, either inter-filament or inter-strand are given in general by [6]:

$$Q_c = \oint P_c dt = \frac{n\tau\pi\omega(B_{max})^2}{\mu_o\left(1 + (\omega\tau)^2\right)} \tag{4}$$

where B_{max}, ω, n, and τ are the peak ripple field amplitude, ripple field angular frequency, the geometric factor, and either the inter-filament coupling time constant or the inter-strand coupling time constant, respectively. For a low ripple frequency ($\omega\tau << 1$), the total coupling loss is given by the sum of inter-filament coupling loss Q_{if} and inter-strand coupling loss Q_{is} as:

$$Q_c = Q_{if} + Q_{is} = \frac{\pi B_{\max}^2 \omega}{\mu_o}\left(n_f \tau_f + n_s \tau_s\right) \tag{5}$$

where τ_f, and τ_s are respectively the inter-filament coupling time constant and inter-strand coupling time constant, and n_f, and n_s are respectively the geometric factors for the inter-filament coupling and inter-strand coupling. The inter-filament coupling-loss geometric factors n_f is assumed to be 2 [7]. The time constants have been given as,

$$\begin{aligned} \tau_f &= \frac{\mu_o}{2\rho_f}\left(\frac{L_f}{2\pi}\right)^2 \\ \tau_s &= \frac{\mu_o}{2\rho_c}\left(\frac{L_s}{2\pi}\right)^2 \end{aligned} \tag{6}$$

here ρ_f, L_f, ρ_c, and L_s are respectively, the effective resistivity of the strand matrix material, twist pitch of the filaments in a strand, the effective transverse resistivity between strands, and the dominant twist pitch (the last stage twist pitch) of the cable.

B. Evaluations of hysteresis loss and inter-filament coupling loss

To evaluate hysteresis loss using (2), B_p was calculated with (3) using the critical current of ITER IGC wire, $I_c = (45.81 - 1.94\ B)^2\ B^{-0.5}$ (A) [8]. The zero field current density was assumed to be 4400 A/mm^2. The effective filament diameter which was evaluated at 3 T by a SQUID hysteresis-loss measurement was $2a = 14.3$ μm [9].

All of the parameters for the inter-filament time constant were known with the exception of the ρ_f. The effective resistivity ρ_f of copper matrix material is known to vary linearly with the magnet field. It is written as:

$$\rho_f = \rho_{f0} + \alpha B \tag{7}$$

In (8) ρ_{f0} is the zero field initial matrix resistivity, B is the applied DC bias field, and the multiplication factor $\alpha = 4.8\text{x}10^{-11}$ Ωm/T. Inter-filament coupling loss Q_{if} can be re-written using (7) as:

$$Q_{if} = \frac{B_{\max}^2 \omega L_f^2}{2\pi(\rho_{f0} + \alpha B)} \tag{8}$$

An unknown parameter of the effective matrix resistivity ρ_{f0} in (8) was evaluated from a reported strand coupling loss data of ITER IGC similar wire. [10]. According to the strand loss data, the coupling time constant τ_f was 2.1 ms assuming the

inter-filament coupling-loss geometric factors n_f is 2. From the time constant value, the zero field initial resistivity ρ_{f0} was evaluated to be 6.7×10^{-10} Ωm at 4.2 K. In this work hysteresis loss and inter-filament coupling loss were evaluated by (2) and (8), respectively.

IV. Test Results and Discussion

The experiments were performed at the NHMFL on two separate cool-downs. At the first cool-down the test operation system including the calorimetric measurement was checked at a DC magnetic field of 3 T with a constant ripple field without a transport current. All of the measurements presented here were obtained at the second cool-down. The AC loss measurements were performed at various DC background fields with/without DC transport currents. The magnet power supply was modulated at 4 Hz to obtain the constant ripple field of B_{max} = 15 mT.

TABLE II

Chronological List of Measurements Performed

Data Sequence	Back Ground DC Field (T)	DC Transport Current (A)	Event Description
1	6	0	At the background field of 6 T without the sample transport currents.
2	12	1.0	At 12 T with the sample transport currents between 1 kA to 4 kA. (There was a quench at the end while trying to increase the sample current up to 4.5 kA. The quench occurred at approximately 4.3 kA.)
3	12	2.5	
4	12	4.0	
5	12	4.0	At 12 T with the sample transport currents between 4 kA to 1 kA.
6	12	2.5	
7	12	1.0	
8	9	4.0	At 9 T with the sample transport currents between 4 kA to 0 kA.
9	9	2.5	
10	9	1.0	
11	9	0	
12	6	4.0	At 6 T with the sample transport currents between 4 kA to 0 kA.
13	6	2.5	
14	6	1.0	
15	6	0	
16	8	6.0	At 8 T with 6 kA transport current.
17	10	4.8	At 10 T with 4.8 kA transport current.
18	9	4.0	At 9 T with 4 kA transport current.
19	10	4.0	At 10 T with 4 kA transport current.
20	12	0	At 12 T without transport current.
21	6	0	At 6 T without transport current.

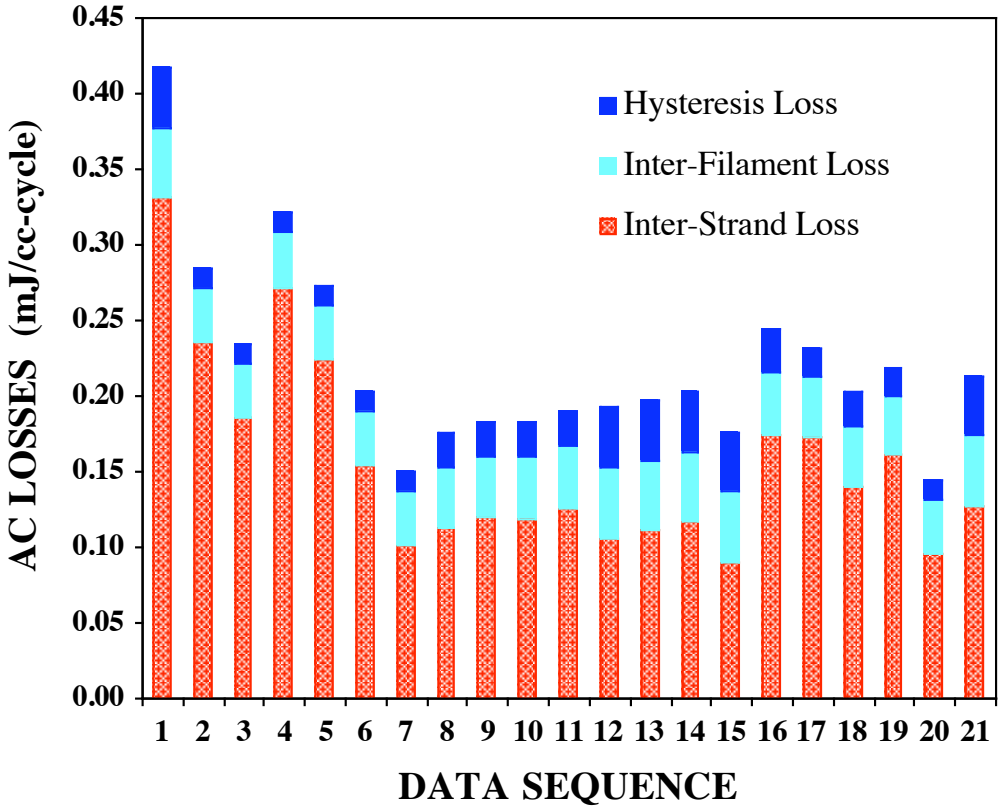

Fig. 3 AC loss results in chronological order measured with the ripple field of the amplitude 15 mT and the frequency 4 Hz under various conditions of background fields and transport currents described in Table II. Calculated hysteresis loss and inter-filament coupling loss are shown by bar graphs for each measurement.

Fig. 3 shows AC loss test results measured under various conditions described in Table II. The test data list in chronological order of the measurements performed. In Fig. 3 bar graphs for each measurement indicate contributions of hysteresis loss and inter-filament coupling loss which were calculated from (2) and (8) as described in the previous section. Fig. 4 shows the coupling effective time constants $n_s\tau_s$ of the inter-strand coupling loss components (Measured total loss - Hysteresis loss - Inter filament coupling loss) were calculated from (5). It was found that over the course of the experiment the effective time constants $n_s\tau_s$ of the inter-strand coupling tended to decrease at the beginning of the test operations, as the similar coupling loss drops have been reported [11]. The effective time constant $n_s\tau_s$ decreased from about 20 ms to approximately 8 ms at zero transport current. The inter-strand coupling loss components of Data Sequence #5 to #21 are shown in Fig. 5 as a function of the cross

product of the transport current and the magnetic field, IxB, which gives Lorentz force of the cable. Individual strand stress in the cable is proportional to the Loren force of IxB. The applied field and transport current for this experiment were assumed to be acting normal to one another. The solid line was the best fit obtained by a computer curve fitting. As seen in Fig. 4 the data of 12 T at 48 kN/m might not yet have reached to equilibrium. However, it is clearly seen in Fig 5 that the inter-strand coupling loss increases with increasing the Lorentz force. It is noted that the increment is very gradual at low Lorentz force region and then sharply increases at 30 kN/m. An increase of Lorentz loading from 0 to 50 kN/m resulted in an 84% increase of the inter-strand coupling loss.

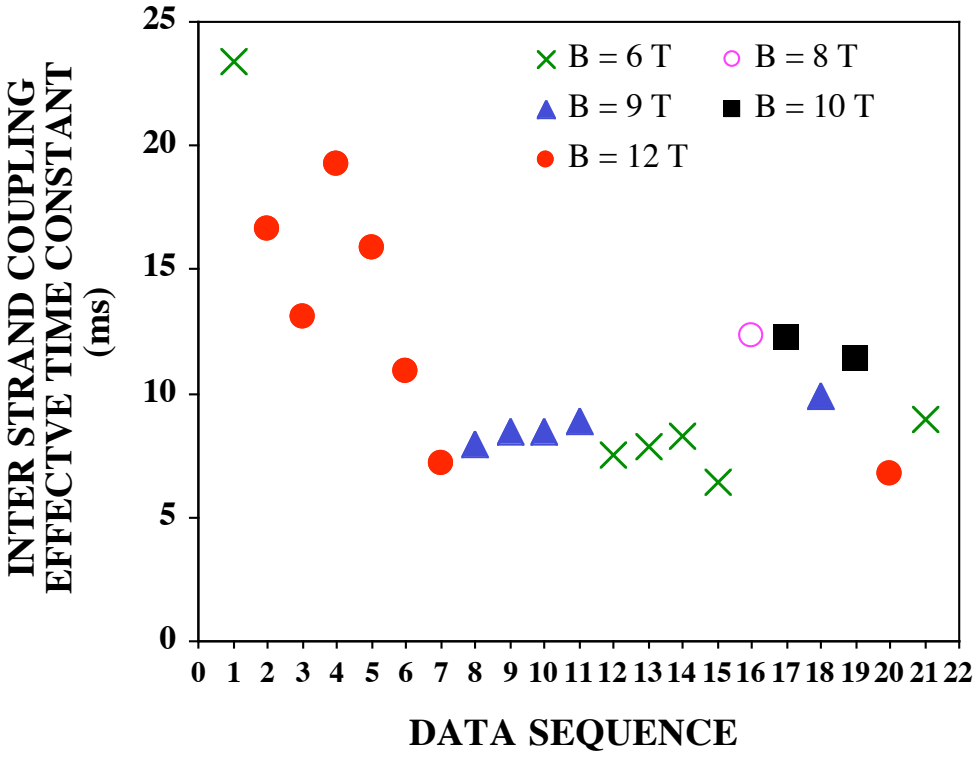

Fig. 4 Coupling effective time constants $n_s t_s$ of the inter-strand coupling loss components (Measured total loss - Hysteresis loss - Inter filament coupling loss) in chronological order taken.

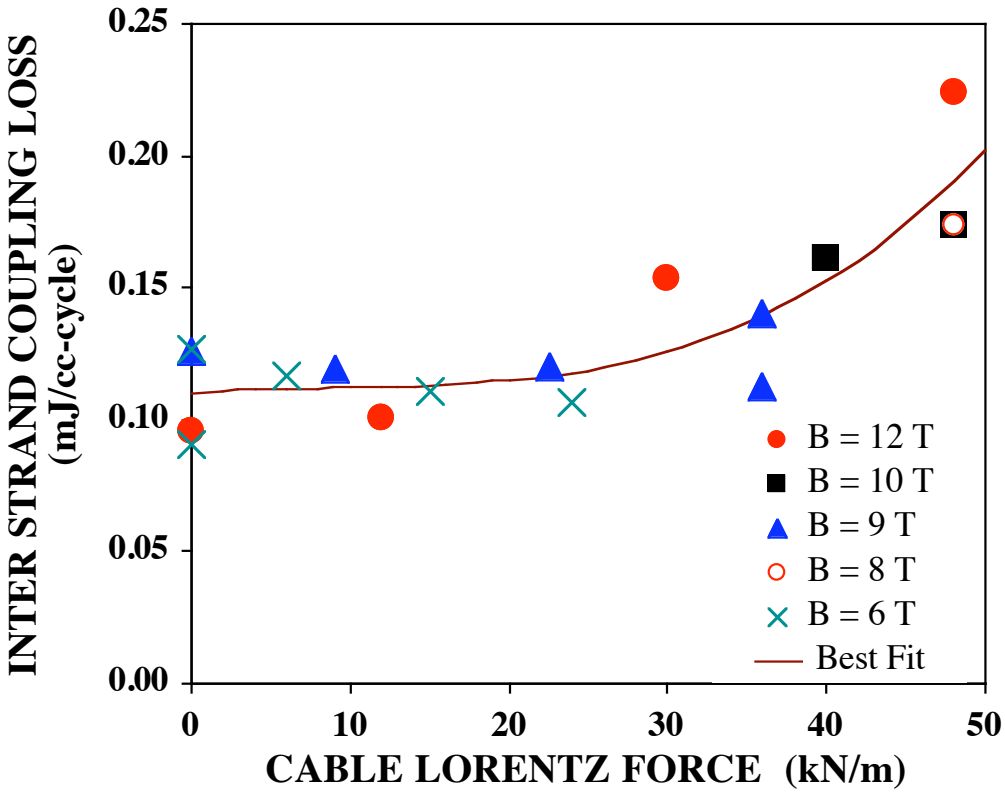

Fig. 5 Inter-strand coupling loss components are plotted as a function of the cable Lorentz force (the transport current x the field).

The transverse resistivity ρ_c between strands which is in (6) of the inter-strand coupling loss has been reported to change with Lorentz force loading IxB in cable [12]. The conductance σ_c (resistivity inverse) between strands varies linearly with the Lorentz force loading. Therefore $1/\rho_c$ is replaced with a linear function that varies with the Lorentz force (IxB) given by:

$$\frac{1}{\rho_c} = \sigma_c = \sigma_i + \beta IB \tag{9}$$

where σ_i, IB, β are the zero-field transverse conductivity, Lorentz force, and a constant parameter unknown, respectively. Inter-strand coupling loss Q_{is} in (5) can be re-written using (6) and (9) as:

$$Q_{is} = \frac{B_{\max}^2 \omega n_s \left(\sigma_i + \beta IB\right) L_s^2}{4\pi} \tag{10}$$

The non-linear behavior of the inter-strand coupling loss vs. IxB in Fig. 5 was not

explained with the linear effect of IxB on transverse conductance. The geometric factor of the inter-strand coupling loss, n_s in (10) could be also a function of Lorentz force. The geometric factor n_s is given as $(1-N_s)^{-1}$ with the demagnetizing factor N_s [7]. The demagnetizing factor N_s of the inter-strand coupling could decrease with increasing Lorentz loading force since Lorentz force squashes the cable in the direction perpendicular to the field. Consequently the geometric factor of the inter-strand coupling loss, n_s, tends to decrease with decreasing N_s. The inter-strand coupling loss could decrease with Lorentz force loading.

With those two contributions; increasing due to the transverse conductance and decreasing due to the geometric factor n_s, the inter-strand coupling loss might increase in a parabolic shape with the Lorentz force factor as seen in Fig. 5.

V. CONCLUSIONS

An experimental study of ripple field AC losses was carried out on a 36-strand sub-sized Cable-In-Conduit-Conductor of Nb_3Sn superconducting wires with transport currents ranging from 0 to 6 kA at various DC background fields using an isothermal calorimetric method. The AC loss measured for this work was dominated by inter-strand coupling loss. Twisted CICC type cables showed a relaxation (training) phenomenon on AC loss at the beginning during operation tests. The effective time constant ($n_s\tau_s$) of the inter-strand coupling loss at zero current declined from about 20 ms to 8 ms.

It was observed that the inter-strand coupling loss depended on the product of the transport current and the magnetic field, IxB, of Lorentz force. The inter-strand coupling loss increased gradually and then sharply at approximately 30 kN/m with increasing Lorentz force loading, and resulted in an 84% increase at the Lorentz force of 50 kN/m. The phenomenon was not explained with only the decrease of contact resistance between strands caused by Lorentz forces. An additional effect of Lorentz force on the geometric factor of the inter-strand coupling loss could be considered. Lorentz force affects on a cable compaction, which results changing the geometric factor of the inter-strand coupling loss since it is a function of the strand demagnetization factor.

ACKNOWLEDGMENT

A special thanks goes to Dr. Chen-Yu Gung and Dr. Philip Michael for all their technical advice. Many thanks go to Mr. Dave Tracey and Mr. Rick Lations for all their help in building the equipment for this work. We are especially thankful to Dr. Bruce Brandt, for all his planning and advice made our visits to the NHMFL successful and so enjoyable. We would like to thank also Dr. Scott Hannahs and Mr. Bobby Joe Pullum for all their help running our experiment at the NHMFL. We also thanks Dr. R.B. Goldfarb, NIST for strand hysteresis loss measurements and helpful discussions.

REFERENCES

[1] R.J. Thome, MT-15, 6-11, 1998.

[2] M. Takayasu, C.Y. Gung, M.M. Steeves, B. Oliver, D. Reisner D, M.O. Hoenig, "Calorimetric measurement of AC loss in Nb_3Sn superconductors," 11th International Conference on Magnet Technology (MT-11), Elsevier Applied Science, 1990, pp.1033-8 vol.2. London, UK.

[3] C.Y. Gung, M. Takayasu, M.M. Steeves, M.O. Hoenig, "AC Loss Measurement of Nb3Sn Wire Carrying Transport Current," *IEEE Trans. Magnetics*, 2,1991,p. 2162.

[4] M.N. Wilson, *Superconducting Magnets*, Oxford University Press, Oxford, (1983).

[5] For example, Y. Iwasa, *Case Studies in Superconducting Magnets*, Plenum Press, New York, (1994).

[6] A. Nijhuis, H.H.J. ten Kate, J.L. Duchateau, P. Bruzzone, "Coupling Loss Time Constants in Full-Size Nb3Sn CIC Model Conductors for Fusion Magnets," Advances in Cryogenic Engineering, vol. 42, Plenum Press, New York, 1281-1288, 1996.

[7] A.M. Campbell, "A General Treatment of Losses in Multifilamentary Superconductors," Cryogenics, vol. 22, pp. 3-16, 1982.

[8] M. Takayasu, A. Childs, R. Randall, R. Jayakumar, J. Minervini, "ITER Niobium-Tin Strands Reacted under Model Coil Heat-Treatment Conditions," *IEEE Trans. App. Superconductivity*, 9,1999, p. 644.

[9] Ron Goldfarb of NIST, Private Communications.

[10] C. Gung, 'ITER Strand Bench Mark Test II: Test Report: Hysteresis Loss of Strand-C," MIT PSFC Memorandum, Reference Number – ITER/US/95/EV-MAG /C.Y.Gung/05.19/-1, May 19, 1995.

[11] A. Nijhuis, N.H.W. Noordman, H.J. ten Kate, N. Mitchell, and P. Bruzzone, "Electromagnetic and Mechanical Characterisation of ITER CS-MC Conductors Affected by Transverse Cyclic Loading, Part 1: Coupling Current Loss," *IEEE Trans. App. Superconductivity*, 9,1999, p. 1069.

[12] M. Takayasu, C.Y. Gung, M.M. Steeves, J.V. Minervini, "Measurements of Transverse Resistance of Multi-Strand Superconducting Cables," Presented at 13th International Conference on Magnet Technology (MT-13), 1993.